



## **Influence of imperfections on the local buckling response of hollow structural shapes**

Joanna Nseir<sup>1</sup>, Marielle Hayeck<sup>2</sup>, Elsy Saloumi<sup>3</sup>, Nicolas Boissonnade<sup>4</sup>

### **Abstract**

The present paper investigates the behavior and response of square and rectangular hollow sections experiencing local buckling. More precisely, the concern is here to characterize in which extent geometrical imperfections may influence the cross-sectional resistance. This is of particular relevance in the context of using advanced F.E. models in practical design, since very little recommendations or guidelines may be found in the literature. Accordingly, the present paper focuses on the influence of geometrical (local) imperfections. The effects of imperfections' shapes, periods and amplitudes are investigated numerically, by means of suitable shell F.E. models. Adequate comparisons with measured data are provided, as well as practical recommendations for a sound F.E. modeling.

### **1. Introduction**

Real initial geometrical imperfections in steel members are in general unknown, especially regarding their magnitudes. A safe but rather unrealistic and over-conservative answer to this question may consist in associating what is assumed to be the most unfavorable shape of the imperfections together with amplitudes given by fabrication tolerances. Such guidelines for modeling initial imperfections of plates are given in the European standards for plated structural elements (EN1993-1-5 2005), which allow to model geometric imperfections together with structural imperfections resulting from welding and/or cutting, as equivalent geometric imperfections with amplitudes given at the allowable fabrication tolerances (see Figure 1). It is recommended to consider relevant imperfection shapes and to determine the most unfavorable combination in terms of leading material or geometrical imperfection with full amplitude and accompanying imperfection with 70% of the amplitude given in Figure 1. In other words, if residual stresses patterns are introduced in the model as the leading imperfections, the accompanying geometrical imperfection amplitude can be lowered to 70% of the amplitude mentioned in Figure 1. Also, Eurocode 3 part 1-5 (EN1993-1-5 2005) allows to model imperfections with 80% of the geometric fabrication tolerances combined with residual stresses

---

<sup>1</sup> PhD, University of Applied Sciences of Western Switzerland, <joanna.nseir@gmail.com>

<sup>2</sup> Graduate Student, University of Applied Sciences of Western Switzerland, <elsysaloumi@gmail.com>

<sup>3</sup> Graduate Student, University of Applied Sciences of Western Switzerland, <marielle\_hayeck@hotmail.com>

<sup>4</sup> Professor, University of Applied Sciences of Western Switzerland, <nicolas.boissonnade@hefr.ch>

represented by a stress pattern from the fabrication process with amplitudes equivalent of the mean expected values.

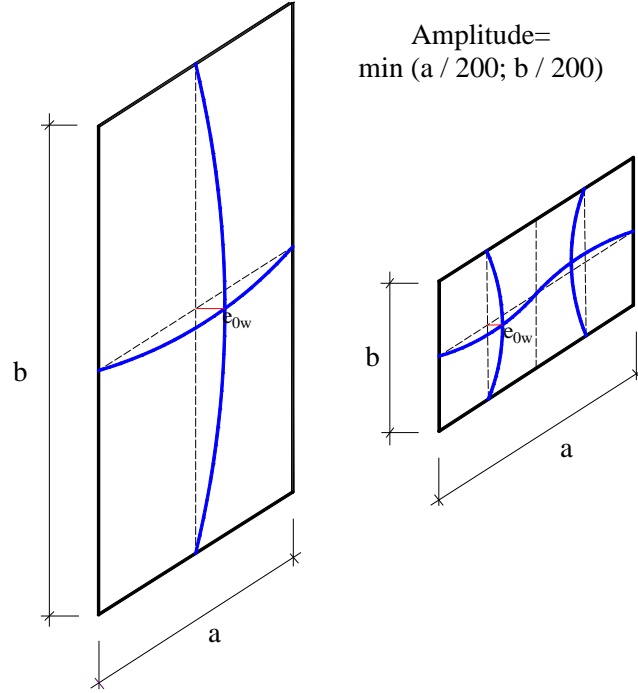


Figure 1: Local imperfections according to Eurocode 3 part 1-5

Kettler (Kettler 2008) introduced local geometrical imperfections through an appropriate modification of node coordinates, obtained from the first eigenmode shape of the corresponding element subjected to axial compression. Greiner et al. (Greiner et al. 2007) adopted a predicted shape of the local buckling mode with the use of a sine shape of initial deformation with appropriate amplitude for each plate, determined separately as a function of the plate's width.

Earlier, Dawson and Walker (Dawson 1972) had suggested an expression to predict the initial imperfection amplitudes in simply supported plates and in the flat parts of square hollow sections. Different generalized geometrical imperfection parameters were studied and their effects were compared to test data obtained from cold-formed steel sections subjected to either bending or compression. A suitable and completely general parameter describing the imperfection's amplitude, of a plate with thickness  $t$ , was derived by means of the following three equations:

$$e_{0,w} = \alpha t \quad (1)$$

$$e_{0,w} = \beta \left( \frac{f_y}{\sigma_{cr}} \right)^{0.5} t \quad (2)$$

$$e_{0,w} = \gamma \left( \frac{f_y}{\sigma_{cr}} \right) t \quad (3)$$

where  $e_{0,w}$  is the initial imperfection amplitude,  $t$  is the plate thickness,  $f_y$  is the yield stress of the material,  $\sigma_{cr}$  is the plate critical buckling stress and  $\gamma$ ,  $\alpha$  and  $\beta$  are constants to be determined for each type of material which are assumed to be influenced by the manufacturing process. For example, Walker (Dawson 1972) recommended a value  $\gamma = 0.2$  for cold-formed steel sections.

To take due account of the variation of edge restraints for various cross-sectional geometries of cold-formed steel members, Walker (Dawson 1972) recommended the use of Eq. (2) with  $\beta = 0.3$ . Cruise and Gardner (Cruise et al. 2006) adopted Dawson and Walker's expression and proposed a value of  $\beta = 0.023$  for cold-rolled stainless steel rectangular hollow sections and replaced the yield stress  $f_y$  with the 0.2% proof stress  $\sigma_{0.2}$ , whereas Jandera et al. (Jandera et al. 2008) suggested a value of 0.045 which lies between the upper (0.111) and lower (0.012) bounds reported by Cruise and Gardner (Cruise et al. 2006).

Unlike almost all existing studies focusing on the sole imperfections' amplitude, Schafer and Pekoz (Schafer et al. 1998) studied both amplitudes and distributions of imperfections, and proposed simple rules of thumb assorted with a probabilistic treatment of the maximum imperfection magnitude as a random variable. Numerically estimated cumulative function C.D.F. values were proposed and served as a basis for associating a probability of occurrence with a particular imperfection magnitude. Schafer also performed an experimental program to assess the proposed imperfection distributions; he used the imperfection spectrum of the experimental program to characterize the imperfection magnitude in a particular eigenmode. Five artificial imperfection signals were generated and the associated patterns were seen to be more complex than those obtained from modal imperfections. In these latter type of imperfections, failure mechanisms were either local or distortional depending on the imperfection magnitude (local and distortional modes were studied), whereas analysis through the generalized imperfections showed that failure was dependent on both magnitude and distribution of imperfections. Moreover, with generalized imperfections, yielding and final failure mechanism occurred at a variety of locations (but eventually at large deflections, an eigenmode shape was formed) whereas a regular failure mechanism was developed with modal imperfections (e.g. distortional failures with distortional modal imperfection).

The research investigations reported in this paper are relative to sensitivity studies conducted on hollow cross-sections, targeting the influence of both the shape and amplitude of initial imperfections, with the objective of providing suitable recommendations for F.E. modelling. Section 2 first details two studies relative to the local imperfection shape: the first one is relative to a comparison between measured local imperfections of tested cross-sections with assumed numerical imperfection shapes, while the second study is relative to further F.E. studies on other cross-sections with various local imperfection shapes. Section 3 focuses on a study related to the amplitude of the initial geometrical imperfections, and section 4 eventually proposes practical recommendations for the introduction of imperfections in the F.E. modeling of hollow cross-sections.

## 2. Influence of geometrical imperfections' shape

### 2.1. Comparison with experimental measurements

The treatment of geometrical imperfections is of significant importance within structural steel, since both ultimate strength and post-buckling response are imperfection-sensitive.

Table 1: Comparison of experimental and numerical results for cold-formed sections according to the different imperfection shapes adopted

Specimen	$\frac{h-2r-t}{200}$ [mm]	$\frac{b-2r-t}{200}$ [mm]	Average [mm]	Denom. of web width <sup>5</sup> [-]	Denom. of flange width [-]	Measured amplitude web [mm]	Measured amplitude flange [mm]	Measured amplitude average [mm]
RHS_LC1_S355CF_200x100x4	0.92	0.42	0.67	287	18	1.56	0.22	0.89
RHS_LC1_S355CF_220x120x6	0.98	0.48	0.73	143	49	0.73	0.52	0.62
RHS_LC1_S355HF_250x150x5	1.16	0.662	0.912	452	104	1.95	0.79	1.37
RHS_LC1_S355HF_200x100x5	0.912	0.412	0.66	140	21	0.77	0.26	0.51
SHS_LC1_S355CF_200x200x5	0.9	0.9	0.9	403	192	2.24	1.07	1.65
SHS_LC1_S355CF_200x200x6	0.88	0.88	0.88	251	327	1.43	1.86	1.64
SHS_LC1_S355HF_200x200x5	0.912	0.912	0.912	102	127	0.56	0.70	0.63
SHS_LC1_S355HF_200x200x6.3	0.889	0.889	0.889	206	46	1.16	0.26	0.71
RHS_LC2_S355CF_200x100x4	0.92	0.42	0.67	255	222	1.39	2.65	2.02
RHS_LC2_S355CF_220x120x6	0.98	0.48	0.73	131	47	0.67	0.49	0.58
RHS_LC2_S355HF_250x150x5	1.16	0.66	0.91	211	521	0.91	3.95	2.43
SHS_LC2_S355CF_200x200x5	0.912	0.912	0.912	280	293	1.54	1.61	1.57
SHS_LC2_S355CF_200x200x6	0.88	0.88	0.88	151	105	0.86	0.6	0.73
SHS_LC2_S355HF_200x200x5	0.912	0.912	0.912	71	76	0.39	0.42	0.40
SHS_LC2_S355HF_200x200x6.3	0.889	0.889	0.889	94	58	0.53	0.33	0.43
RHS_LC3_S355CF_200x100x4	0.92	0.42	0.67	667	95	3.63	1.14	2.39
RHS_LC3_S355CF_220x120x6	0.98	0.48	0.73	780	18	3.98	0.19	2.08
RHS_LC3_S355HF_250x150x5	1.16	0.66	0.91	728	327	3.14	2.48	2.81
RHS_LC3_S355HF_200x100x5	0.91	0.41	0.66	242	14	1.33	0.18	0.75
SHS_LC3_S355CF_200x200x5	0.9	0.9	0.9	279	160	1.55	0.89	1.22
SHS_LC3_S355CF_200x200x6	0.88	0.88	0.88	128	116	0.73	0.66	0.69
SHS_LC3_S355HF_200x200x5	0.912	0.912	0.912	102	206	0.56	1.13	0.84
SHS_LC3_S355HF_200x200x6.3	0.889	0.889	0.889	90	176	0.51	0.99	0.75
2_SHS_LC1_S355CF_200x200x6*	0.88	0.88	0.88	132	177	0.75	-1.01	0.88
2_SHS_LC2_S355CF_200x200x6*	0.88	0.88	0.88	163	230	0.93	1.31	1.12
2_SHS_LC3_S355CF_200x200x6*	0.88	0.88	0.88	158	91	0.90	0.52	0.71
RHS_LC4_S355CF_220x120x6	0.98	0.48	0.73	350	108	1.79	1.13	1.46
RHS_LC5_S355CF_220x120x6	0.98	0.48	0.73	127	69	0.65	0.72	0.68
RHS_LC6_S355CF_220x120x6	0.98	0.48	0.73	129	26	0.66	0.28	0.47
RHS_LC4_S355CF_200x100x4	0.92	0.42	0.67	493	158	2.68	1.89	2.28
RHS_LC5_S355CF_200x100x4	0.92	0.42	0.67	154	31	0.84	0.37	0.60
RHS_LC6_S355CF_200x100x4	0.92	0.42	0.67	180	45	0.98	0.54	0.76
RHS_Stub_S355CF_200x100x4	0.92	0.42	0.67	299	321	1.63	3.83	2.73
RHS_Stub_S355CF_220x120x6	0.98	0.48	0.73	295	24	1.51	0.26	0.88
RHS_Stub_S355HF_250x150x5	1.16	0.66	0.91	74	221	0.32	1.68	1
RHS_Stub_S355HF_200x100x5	0.912	0.412	0.662	238	205	1.31	2.49	1.9
SHS_Stub_S355CF_200x200x5	0.9	0.9	0.9	430	342	2.39	1.9	2.14
SHS_Stub_S355CF_200x200x6	0.88	0.88	0.88	688	255	3.91	1.45	2.68
SHS_Stub_S355HF_200x200x5	0.9125	0.9125	0.9125	405	315	2.22	1.73	1.97
SHS_Stub_S355HF_200x200x6.3	0.889	0.889	0.889	39	51	0.22	0.29	0.25

\* indicates repeated tests

In a first attempt to examine the influence of local imperfection on the cross-section resistance of hollow shapes, an experimental study on the influence of different shapes and amplitudes of initial local geometrical imperfections on the cross-section capacity of some 41 square and rectangular sections was undertaken (Nseir 2015). The tests consisted in hot-finished and cold-formed square and rectangular cross-sections subjected to simple and combined load cases

<sup>5</sup> 'Denom. of web width' refers to the *denominator* in the ratio ' $h-2r-t / denominator$ ' equation which is such that this ratio is equal to the measured maximum amplitude.

(Nseir 2015). The main objective is here to compare different arbitrary initial shapes with the measured imperfections of the experimental tests. Subsequently, the imperfection sensitivity to the expected magnitude can be accurately assessed. Table 1 reports the results of experimental measurements on plates (i.e. webs and flanges) maximum out-of-flatness imperfections.

A series of F.E. calculations was then carried out on all the 41 tested cross-sections (Nseir 2015) with the imperfections and amplitudes mentioned in Figure 2, and the ultimate loads were compared with the experimental results. The cross-section tests had pinned end conditions. The load was applied at the center of rotation of the hinge – represented through truss elements connecting the center of the hinge to rigid endplates at extremities (Nseir 2015). All F.E. calculations comprised measured geometrical dimensions, material laws and residual stresses (Nseir 2015). The only varying parameter was the initial geometrical imperfection as shown in Figure 2. Two main types of imperfections were considered:

- (i) Type I: imperfections introduced through an appropriate modification of node coordinates with adequate sine waves (i.e. sinusoidal wavelength patterns) distributions in both directions of the considered plate. The adopted amplitudes are illustrated in Figure 2 for each plate element individually;
- (ii) Type II: modal imperfections based on the first eigenmode of a linear buckling analysis with scaled amplitude taken as the average of  $h / 200$  and  $b / 200$ , where  $h$  and  $b$  are the web width and the flange width of the section, respectively.

Type I allowed three different variables to define the sine period (case (a), case (b), case (c)). Case (a) consisted of a sine wave imperfection with a period equal to the bigger plate width of the section, case (b) to the smaller plate width of the section and case (c) to the average of both constitutive plates of the section. Case (d) is relative to Type II imperfections.

It is to be noted that the adopted amplitudes corresponded to the prescribed amplitude in EN 1993-1-5 (EN1993-1-5 2005) without a reduction of 30%, although the residual stress patterns were introduced in the calculations. The amplitudes are therefore considered as conservative values.

Figure 3 and Figure 4 show examples of the different initial geometrical imperfections considered for the rectangular cross-section RHS 200x100x4, introduced through adequate sine functions in both directions of each plate, with respect to the periods and amplitudes represented in Figure 2. Figure 4 illustrates the different eigenmode shapes corresponding to the different load cases (LCs) considered in the experimental test series for the RHS 200x100x4 (Nseir 2015).

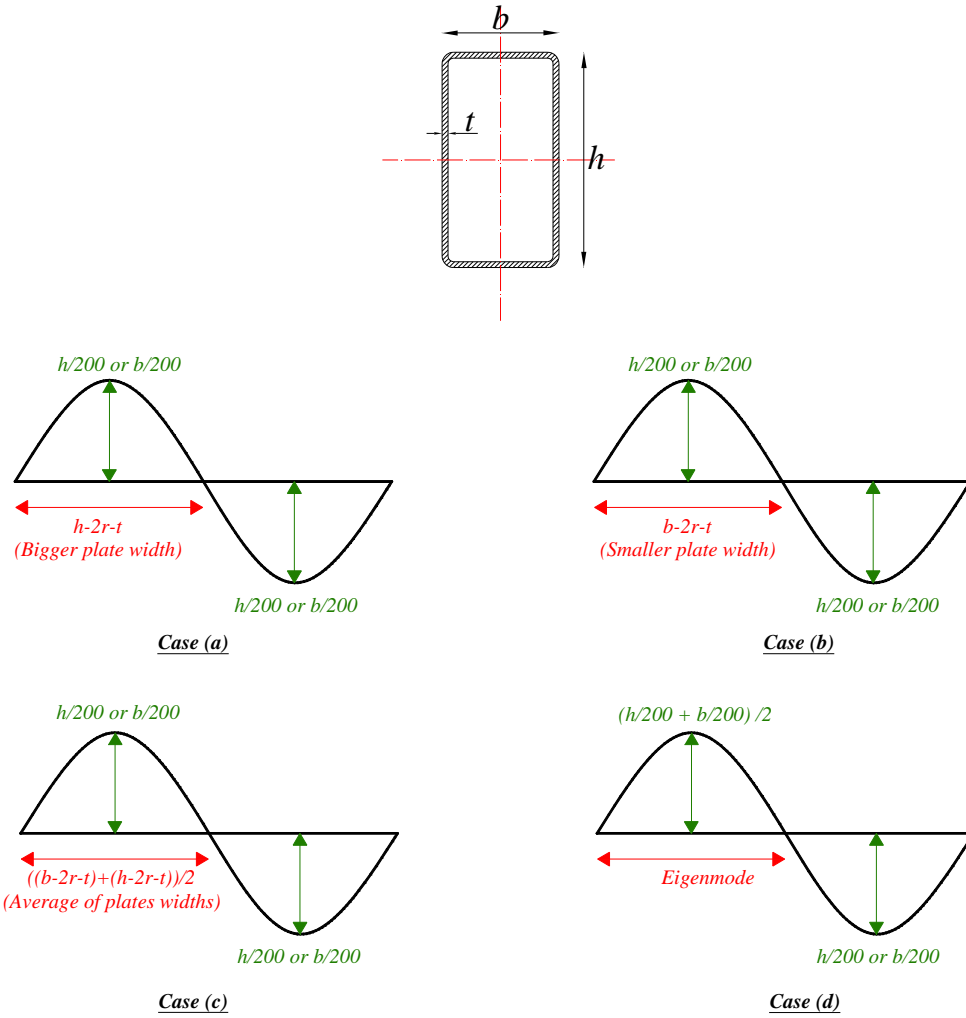


Figure 2: Adopted imperfections for the 41 plated tests

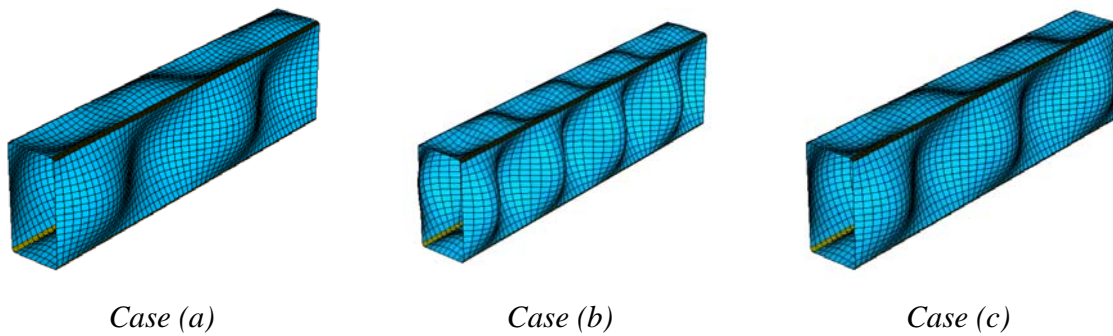


Figure 3: Initial imperfections introduced 'by hand' for the RHS 200x100x4 specimen

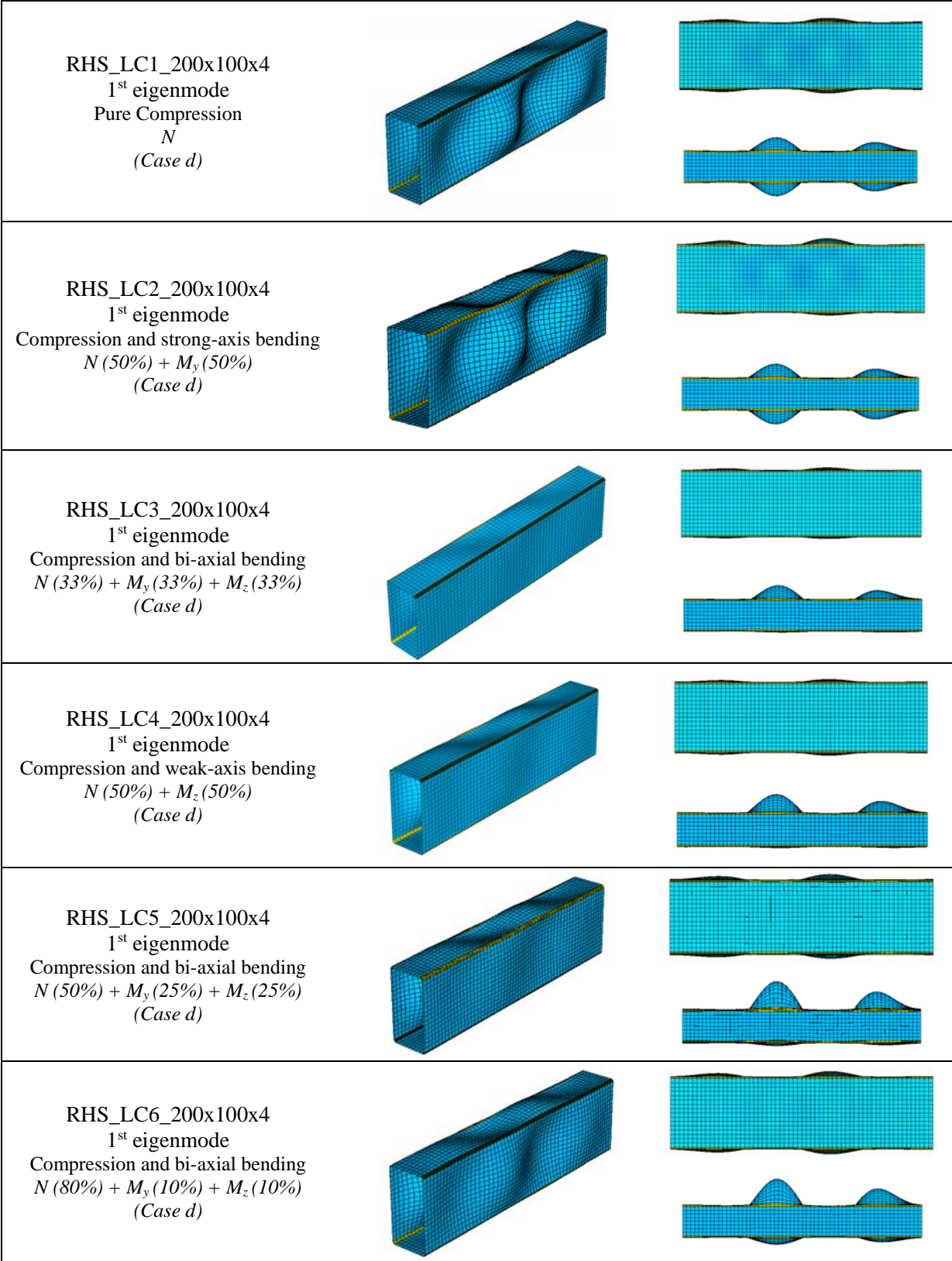


Figure 4: Different imperfections of specimen RHS 200x100x4 introduced through the first buckling mode

Figure 5 to Figure 8 show a comparison of the cross-section capacities having different imperfection patterns with respect to their experimental counterparts. F.E. results including measured imperfections (both amplitudes and patterns) are also included in the comparisons. Figure 5 represents the results corresponding to the cold-formed cross-sections, Figure 6 represents the hot-finished cross-section tests, Figure 7 the cold-formed stub columns and Figure 8 the hot-finished stubs columns. Each figure is accompanied by a corresponding table (see Table 2 to Table 5) in which results are presented as comparative ratios with the experimental results kept as a reference.

The following conclusions can be drawn from these figures:

- (i) The results show relatively minor differences between all the adopted initial imperfections and the experimental reference ones. Nevertheless, this difference is expected to decrease due to the conservative amplitudes in which the reduction of 30% due to the introduction of the residual stresses was not accounted for;
- (ii) Cross-section capacities with measured imperfections were obviously the closest to the experimental results. Then, amongst all remaining imperfection patterns, Type II leads to the closest results to the experimental counterparts in almost all cases, whereas case (b) was the furthest from the experimental results. This was expected since the wave lengths in that case are numerous due to the adoption of the period of the smallest plate width, leading to a drop in cross-section capacity compared to cases (a) and (c) in which the periods were deemed more reasonable;
- (iii) The results showed that case (a) in which the period of the sine wave corresponds to the bigger plate width is closer to the ‘eigenmode imperfection’ result.

Table 2: Comparison of experimental and numerical results for cold-formed sections according to the different imperfection shapes adopted

	$R_{FE\_bigger\ plate}$ / $R_{test}$ [-]	$R_{FE\_smaller\ plate}$ / $R_{test}$ [-]	$R_{FE\_average}$ / $R_{test}$ [-]	$R_{FE\_eigenmode}$ / $R_{test}$ [-]	$R_{FE\_measured}$ / $R_{test}$ [-]
SHS_LC1_200x200x6	0.99	0.99	0.99	1.01	1.02
RHS_LC1_200x100x4	1.05	1.03	1.03	1.05	1.03
RHS_LC1_220x120x6	0.97	0.95	0.95	0.99	1.03
RHS_LC1_200x200x5	0.92	0.92	0.92	0.94	1.05
RHS_LC1_200x200x6	0.91	0.91	0.91	0.94	1.01
RHS_LC2_200x200x6_2	0.91	0.91	0.91	0.93	1.05
RHS_LC2_200x100x4	0.95	0.89	0.91	0.95	1.00
SHS_LC2_200x200x6	0.96	0.96	0.96	0.98	1.03
RHS_LC2_220x120x6	0.91	0.87	0.88	0.92	1.02
RHS_LC2_200x200x5	0.90	0.90	0.90	0.94	1.03
RHS_LC3_200x200x6_2	0.96	0.96	0.96	0.95	1.01
RHS_LC3_200x100x4	0.98	0.94	0.97	0.97	0.97
RHS_LC3_220x120x6	0.95	0.91	0.92	0.95	1.01
RHS_LC3_200x200x5	0.89	0.89	0.89	0.90	1.03
SHS_LC3_200x200x6	0.92	0.92	0.92	0.91	1.03
RHS_LC4_200x100x4	0.96	1.01	1.01	0.94	1.00
RHS_LC4_220x120x6	0.94	0.90	0.91	0.96	1.00
RHS_LC5_200x100x4	0.92	0.89	0.90	0.92	0.97
RHS_LC5_220x120x6	0.93	0.89	0.90	0.94	1.04
RHS_LC6_200x100x4	0.98	0.95	0.95	0.98	1.01
RHS_LC6_220x120x6	0.91	0.88	0.89	0.93	0.96

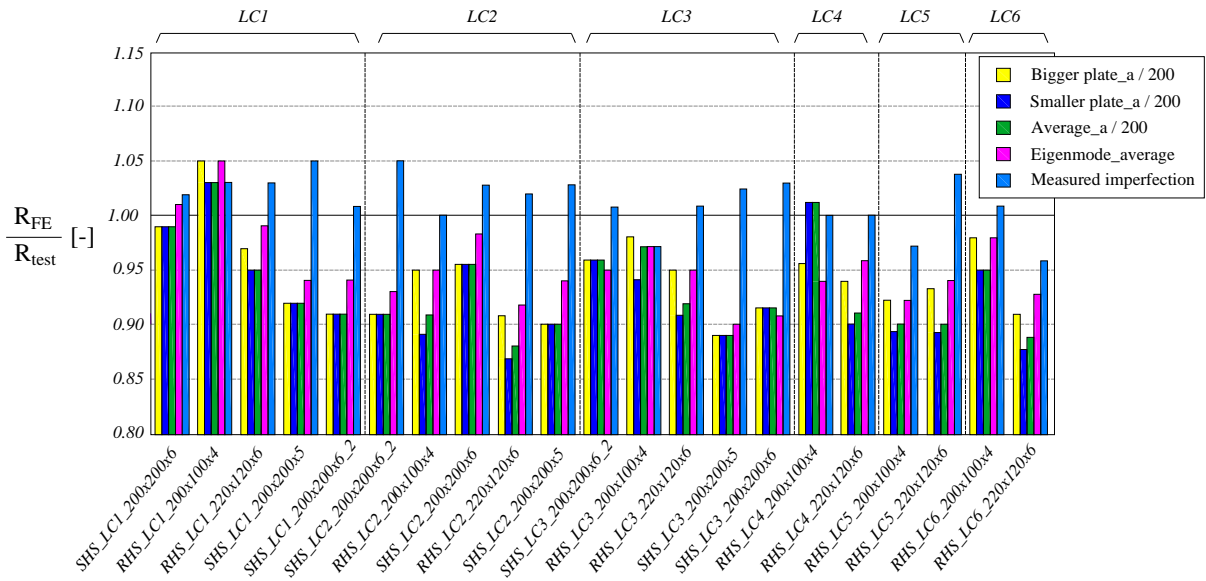


Figure 5: Ultimate results for cold-formed sections according to the different adopted imperfections' shapes

Table 3: Comparison of experimental and numerical results of hot-finished sections according to the different imperfections adopted

	$R_{FE\_bigger\ plate}$ / $R_{test}$ [-]	$R_{FE\_smaller\ plate}$ / $R_{test}$ [-]	$R_{FE\_average}$ / $R_{test}$ [-]	$R_{FE\_eigenmode}$ / $R_{test}$ [-]	$R_{FE\_measured}$ / $R_{test}$ [-]
RHS_LC1_200x100x5	1.00	0.93	0.96	1.01	0.99
RHS_LC1_250x150x5	1.00	0.92	0.95	1.00	1.01
RHS_LC1_200x200x5	0.92	0.92	0.92	0.96	1.00
RHS_LC1_200x200x6.3	0.95	0.95	0.95	0.97	0.99
RHS_LC2_250x150x5	1.02	0.94	0.97	1.01	0.99
RHS_LC2_200x200x5	0.95	0.95	0.95	0.98	0.99
RHS_LC2_200x200x6.3	0.92	0.92	0.92	0.93	0.98
RHS_LC3_200x100x5	1.02	0.96	1.01	1.02	1.00
RHS_LC3_250x150x5	0.94	0.88	0.90	0.92	1.05
RHS_LC3_200x200x5	0.87	0.87	0.87	0.86	0.98
RHS_LC3_200x200x6.3	0.94	0.97	0.97	0.96	1.01

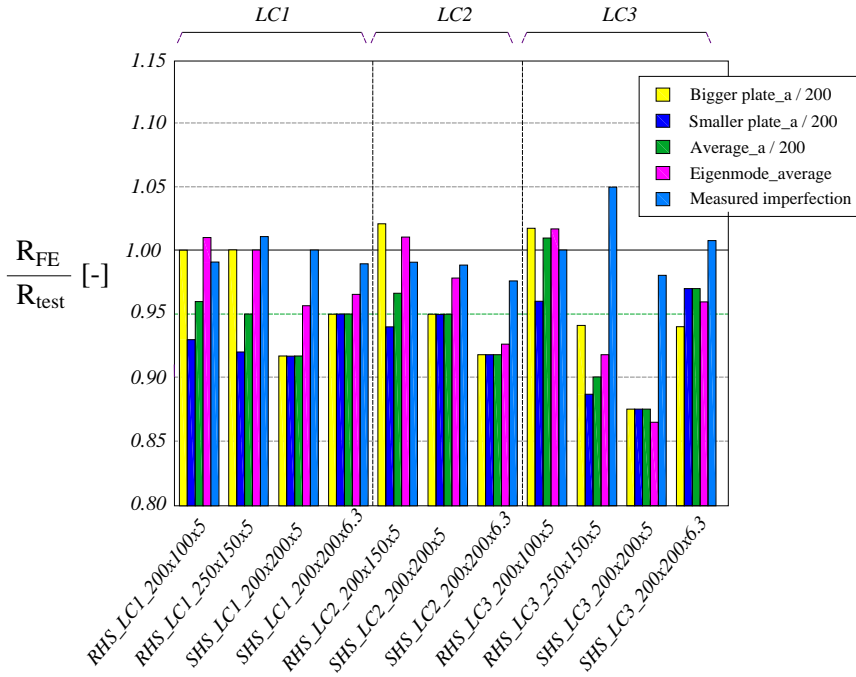


Figure 6: Ultimate results for hot-finished sections according to the different adopted imperfections' shapes

Table 4: Comparison of experimental and numerical results for cold-formed stub columns according to the different adopted imperfections' shapes

	$R_{FE\_bigger\ plate} / R_{test} [-]$	$R_{FE\_smaller\ plate} / R_{test} [-]$	$R_{FE\_average} / R_{test} [-]$	$R_{FE\_eigenmode} / R_{test} [-]$	$R_{FE\_measured} / R_{test} [-]$
RHS_Stub_200x100x4	1.06	1.02	1.03	1.05	1.04
RHS_Stub_220x120x6	0.98	0.92	0.92	0.96	0.93
RHS_Stub_200x200x5	0.93	0.93	0.93	0.92	1.01
RHS_Stub_200x200x6	1.01	1.01	1.01	1.00	1.02

Table 5: Comparison of experimental ultimate load factor with ultimate load factors for hot-finished stub columns according to the different adopted imperfections' shapes

	$R_{FE\_bigger\ plate} / R_{test} [-]$	$R_{FE\_smaller\ plate} / R_{test} [-]$	$R_{FE\_average} / R_{test} [-]$	$R_{FE\_eigenmode} / R_{test} [-]$	$R_{FE\_measured} / R_{test} [-]$
RHS_Stub_250x150x5	1.04	0.95	0.98	1.03	1.02
RHS_Stub_200x100x5	1.02	0.93	0.95	1.00	1.00
RHS_Stub_200x200x5	0.94	0.94	0.94	0.93	1.00
RHS_Stub_200x200x6.3	0.91	0.91	0.91	0.90	0.98

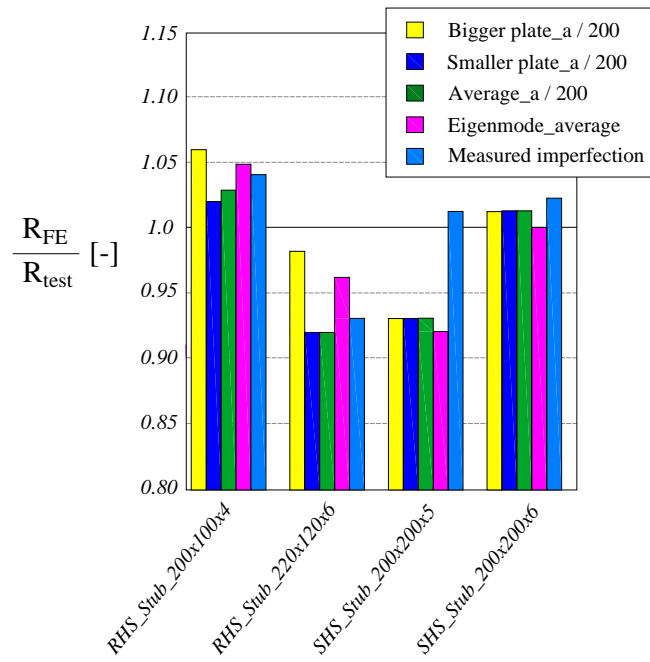


Figure 7: Ultimate results for hot-finished stub columns according to the different adopted imperfections' shapes

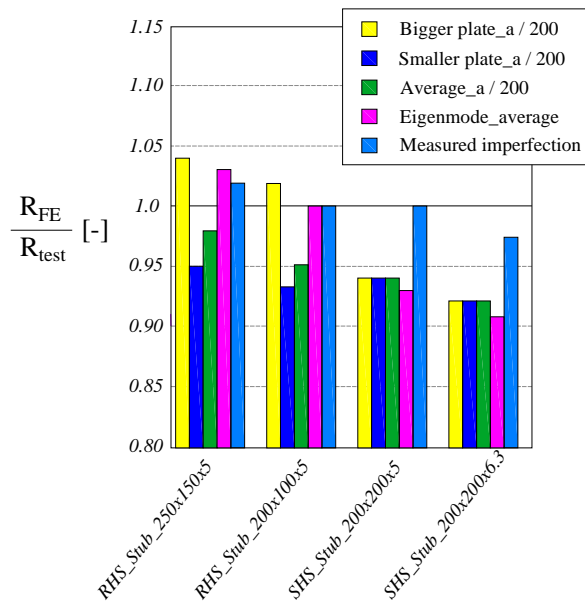


Figure 8: Ultimate results for hot-finished stub columns according to the different adopted imperfections' shapes

## 2.2. Further F.E. studies on different cross-section dimensions – Influence of imperfection shape

A wider study has been conducted on hot-rolled cross-sections with various dimensions and plates' slenderness, considering two simple load cases: axial compression and major-axis bending. The adopted numerical model herein consisted in the use of the linear constraints (see Nseir 2015); sections from all classes (i.e. from plastic to slender) were selected, along with a wider variety of initial imperfections cases, as shown in Figure 9.

Five different types of periods were considered:

- (i) *Average*, referring to a sine period equal to the average of  $(h - 2r - t)$  and  $(b - 2r - t)$ ;
- (ii) *Per plate*, referring to a sine period for each plate considered individually i.e.  $(h - 2r - t)$  or  $(b - 2r - t)$ ;
- (iii) *Smaller*, referring to a sine period with the smallest plate (i.e.  $b - 2r - t$ ) leading all plates of the section;
- (iv) *Bigger*, referring to a sine period with the biggest plate (i.e.  $h - 2r - t$ ) leading all the plates of the section;
- (v) *Eigenmode*, referring to the first eigenmode shape from a linear buckling analysis.

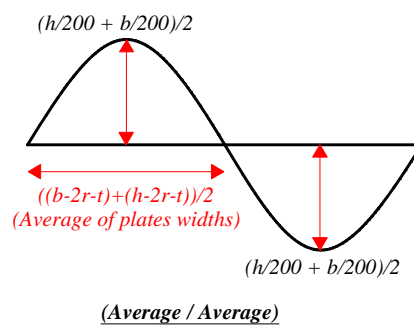
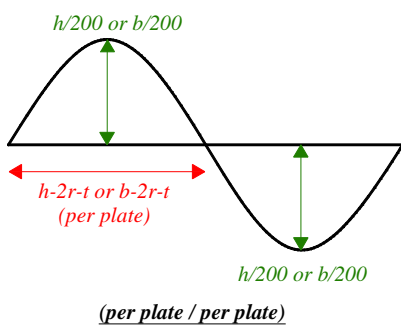
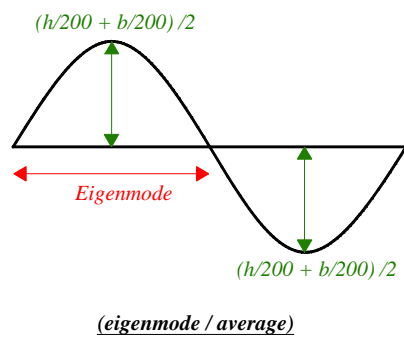
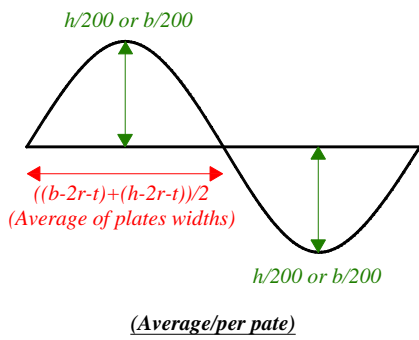
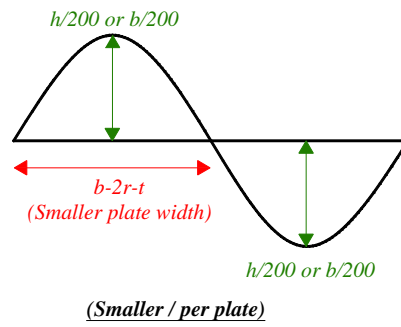
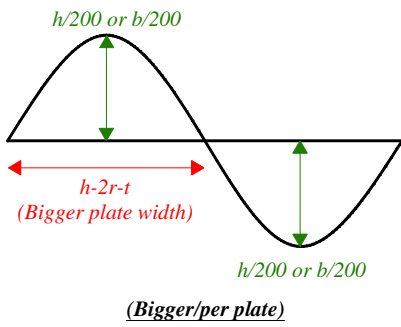
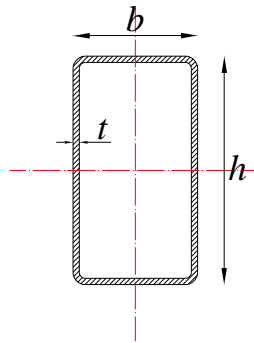
Besides, four different  $a$  values were studied for the definition of the 'imperfection width'  $a$  to define the imperfections' amplitude, according to the format ' $a / 200$ '<sup>6</sup>:

- (i) *Average* refers to an ' $a$ ' equal to  $[(h - 2r - t) + (b - 2r - t)] / 2$ ;
- (ii) *Per plate* refers to an ' $a$ ' equal to  $(h - 2r - t)$  or  $(b - 2r - t)$ ;
- (iii) *Bigger* refers to an ' $a$ ' equal to  $(h - 2r - t)$ ;
- (iv) *Smaller* refers to an ' $a$ ' equal to  $(b - 2r - t)$ .

The case name was divided into two parts; the first part indicates the period of the sine wave and the second part the plate width considered as  $a$  to set an imperfection amplitude  $a / 200$ . Indeed, when considering the cross-section as a whole, not only the imperfections' period shall be fixed (see above), but also the reference plate to be assumed as governing the cross-section's response so as to be used in the determination of  $a$ 's value. For example, in 'smaller/per plate', 'smaller' refers to a period based on the smaller plate width, and 'per plate' refers to an amplitude  $a / 200$  in which  $a$  stands for the corresponded plate width, as explained in the previous section.

---

<sup>6</sup> In the present section, a  $1 / 200$  fraction of  $a$  was fixed for consistency. Different values are considered in section 3.



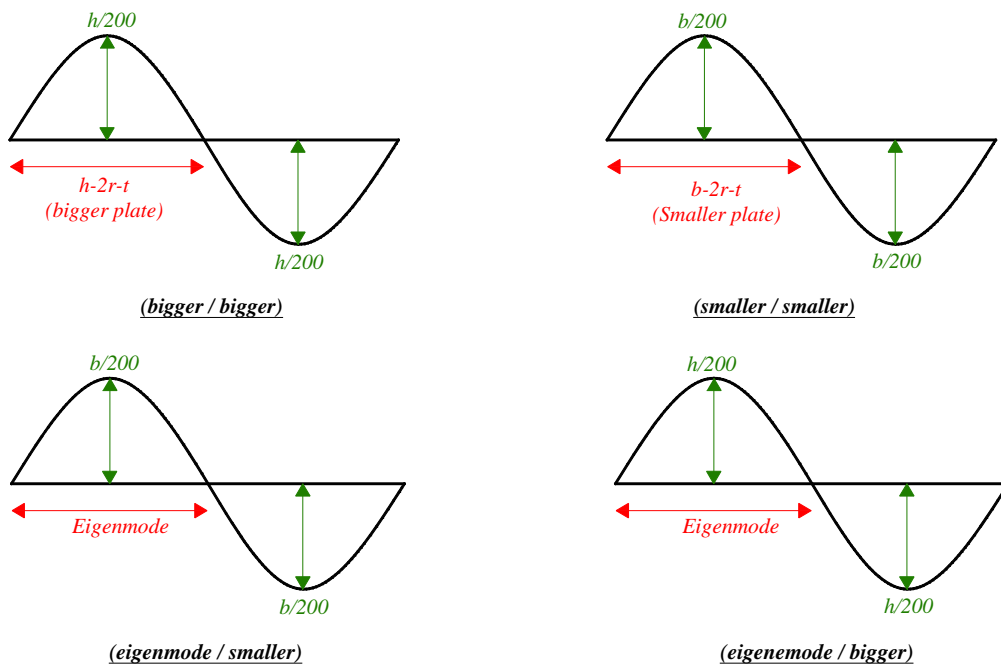


Figure 9: Adopted imperfection shapes

Figure 10 and Figure 11 provide the obtained results, for compression and major-axis bending load cases, respectively. In the vertical axes of Figure 10 and Figure 11, the ultimate compression load and the ultimate bending load were normalized to their respective plastic counterparts (i.e.  $N_u / N_{pl}$  and  $M_u / M_{pl}$ ). The cross-section class of the chosen profiles is also reported in the horizontal axis as indicative information. The imperfection study reveals that:

- (i) The cross-sections subjected to a major-axis bending are less sensitive to the adopted type of imperfection than the cross-sections subjected to compression. The highest difference between the most favorable imperfect shape and the least favorable one in the case of pure compression is about 11%, and is reached for class 3 “semi-compact” sections which are known to be quite sensitive to imperfections (unlike class 1, 2, 4 and 4+ cross-sections). However, in the major-axis bending load case, this percentage reaches a value of only 2%;
- (ii) The ‘eigenmode’ cases led to the highest capacities for the pure compression case and to the lowest for the major-axis bending case. This is mainly due to the unfavorable shape of the ‘eigenmode’ in the bending load cases in which the compression flange has many buckling waves but the tension flange has barely an imperfection; in contrast the imperfection shapes introduced through sine curves in all the plates, including the tension flange, are found to be favorable to this particular load case, given that the sine waves introduced in the tension flange will delay the moment where the tension flange will become thus effective. The ‘eigenmode’ imperfect shape for compression is found to be the least unfavorable one, because the sine periods bear the highest periodicities in comparison to the other imperfect shapes introduced by means of sine curves;
- (iii) Class 1 (plastic) cross-sections are the least affected by the geometrical imperfections in any case considered in this study;

- (iv) In the case of compression load cases, the most unfavorable imperfect shape is revealed to be the case of *smaller/per plate* because of the many buckles in the bigger and smaller plate of the section, in comparison to other imperfect shapes. This phenomenon is accentuated for cross-sections with higher  $h/b$  ratios (see Nseir 2015);
- (v) Eventually, different groups of imperfect shapes are seen to have an almost similar effect on the cross-section capacity. Therefore, the imperfect shapes of *bigger/per plate*, and *bigger/bigger* are seen to have almost equivalent effect on the cross-section capacity as well as for the imperfect shapes of *average/per plate* and *average/average*. The leading parameter in the imperfection shape adoption thus seems to be the period of the sine wave and not its amplitude, as long as this amplitude is taken as a factor of width  $a/200$ , 'a' being the average or exact widths of the plates constituting the section.

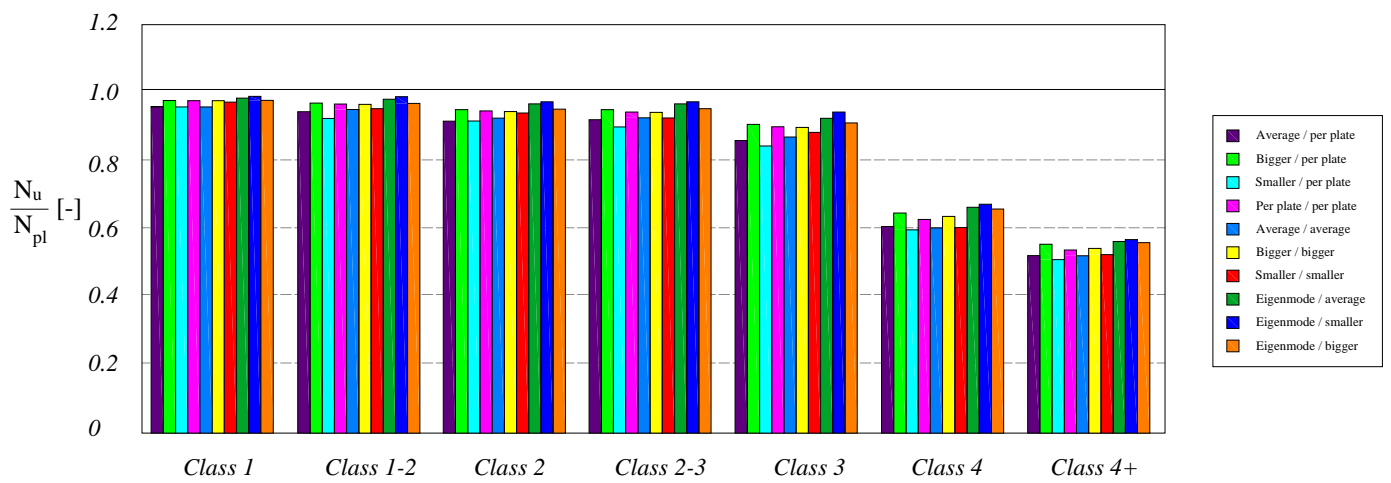


Figure 10: Ultimate results of cross-sections subjected to compression according to the different adopted imperfections

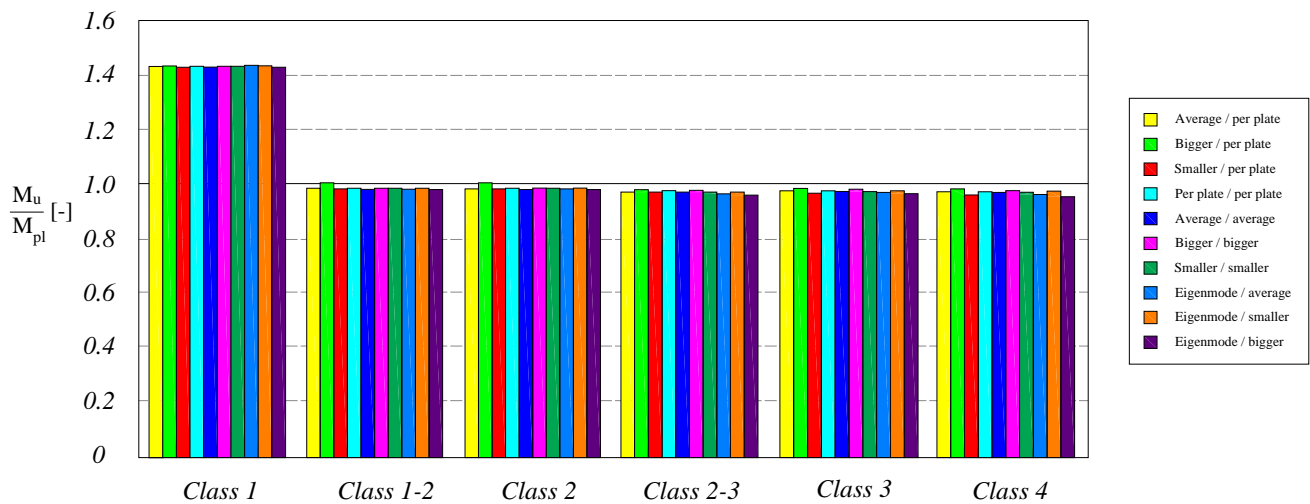


Figure 11: Ultimate results of cross-sections subjected to major-axis bending according to the different adopted imperfections

### 3. Influence of geometrical imperfections' amplitude

A consecutive numerical study was conducted to investigate the effect of the imperfection *amplitude*. The main target was to vary the denominator value (i.e. the value '200' in the  $a/200$  amplitude value) while maintaining the nominator equivalent to each plate width (i.e. factor  $a$ ). Four different amplitudes were adopted:  $a/100$ ,  $a/200$ ,  $a/300$  and  $a/400$ . Some 600 additional F.E. numerical results were obtained for rectangular sections with a  $h/b$  ratio equal to 1.5. Again, two simple load cases were adopted: compression and major-axis bending. The results are shown in Figure 12 and Figure 13, in which horizontal axes provide relative cross-section resistance with respect to the plastic capacity, while horizontal axis represent the cross-section relative slenderness parameter  $\lambda_{CS}$  which is an indicator of the overall cross-section response to the resistance-instability interaction.

The figures show that:

- (i) The stocky and slender cross-sections are less sensitive to the imperfection amplitude;
- (ii) The amplitude of  $a/100$  is the most unfavorable amplitude but is considered too severe to be adopted in F.E. calculations;
- (iii) The differences between various amplitudes considered hardly increase with decreasing amplitudes. Therefore the difference between the curves with  $a/200$ ,  $a/300$  and  $a/400$  becomes less pronounced once the amplitude decreases.

Through this study, the effect of the imperfection amplitude is seen to have a non-negligible impact on a structural response, and has quantitatively as much influence as the sinewaves' periodicities investigated in section 2.

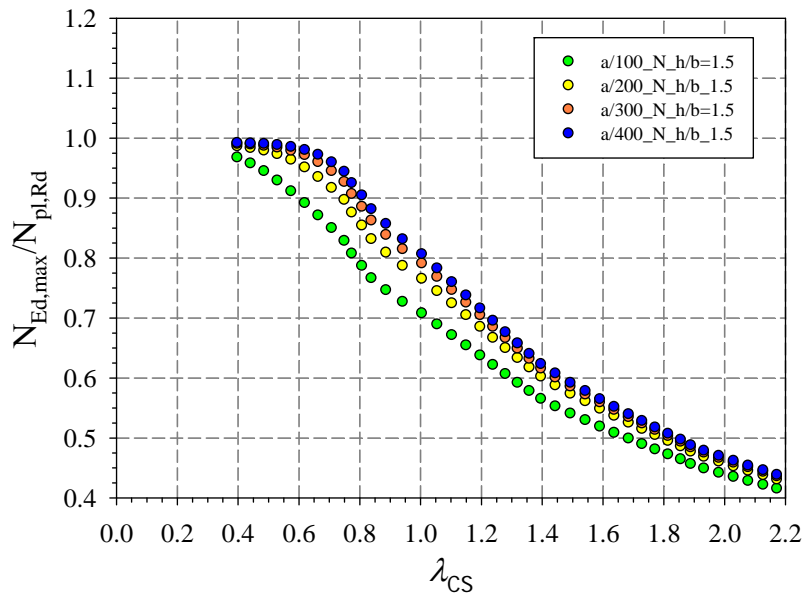


Figure 12: RHS cross-section capacities subjected to pure compression for different imperfections' amplitude

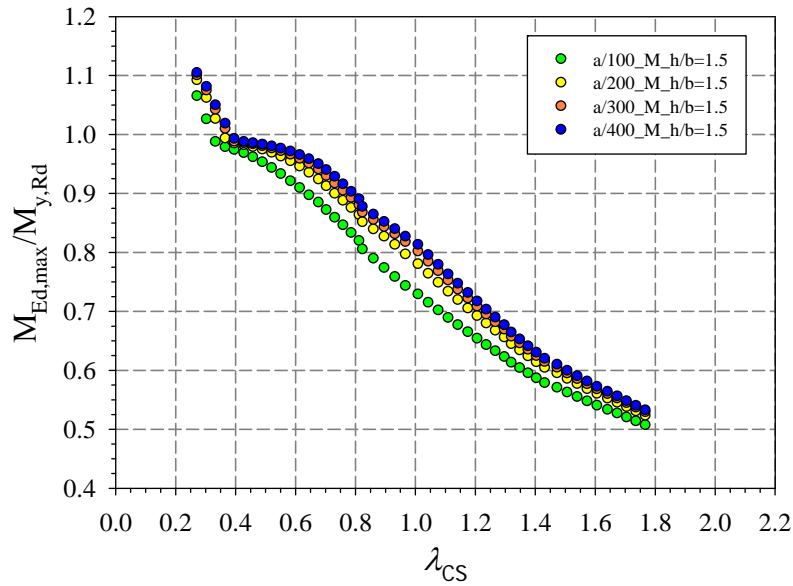


Figure 13: RHS cross-section capacities subjected to major-axis bending for different imperfections' amplitude

#### 4. Summary of observations and recommendations for F.E. modelling

In accordance with previous studies and conclusions, the type and magnitude of imperfections that shall be recommended in the F.E. modelling of square and rectangular hollow structural shapes is as follows:

- (i) Periodicity: average of plate widths;
- (ii) Magnitude:  $a / 200$ ,  $a$  being the depth of the corresponding plate.

Although being quite widely used, the approach consisting in introducing imperfection patterns by means of the first buckling mode was seen to be less appropriate, mainly for load cases other than the pure compression ones (see also Nseir 2015), and does not guarantee safer, conservative results. Therefore, initial geometrical imperfections can be basically introduced through adequate modifications of node coordinates. An example is shown in Figure 14 where local geometrical imperfections have been defined as half-wave patterns in both directions of the flanges and webs.

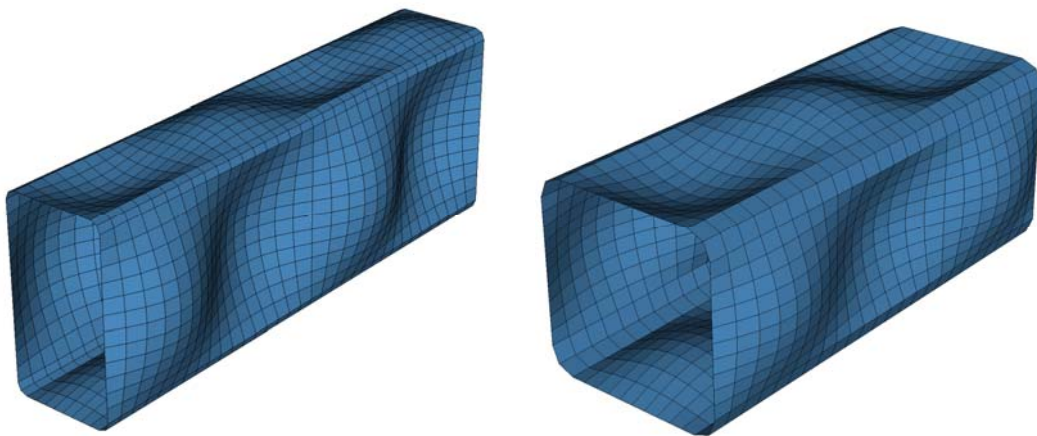


Figure 14: Local geometrical imperfections adopted for square and rectangular hollow sections (magnified view)

It is to be noted that the definition of the sine waves periods must be made dependent of both the web and flanges widths, so that rectangular sections can possess the same number of half-waves in both webs and flanges. Thus, the local imperfections in the flanges and webs will be continuous and coherent, with the corner remaining unaffected, i.e. if the web buckles in an outward direction, the flanges' buckles should be inward and vice versa, as shown in Figure 15.

The following equation has been used accordingly:

$$period = \frac{(h-t-2r) + (b-t-2r)}{2} \quad (4)$$

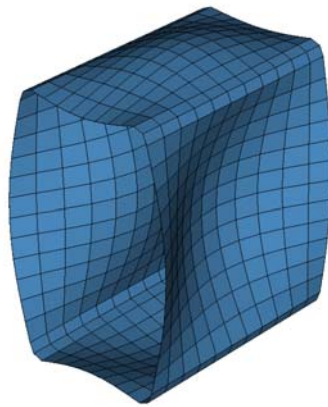


Figure 15: Half sine-wave in a rectangular cross-section

## 5. Conclusions

In the present paper, sensitivity studies relative to initial local geometrical imperfections were undertaken for hollow cross-sections. The aim was to investigate the influence of geometrical imperfection shapes and amplitude on the behavior of hollow sections. The results of hundreds of non-linear shell F.E. calculations are reported and the influence of initial geometrical imperfections is compared.

First of all, a study of the influence of different shapes and amplitudes of initial local geometric imperfections on the cross-section capacity of square and rectangular sections was undertaken, and compared to experimental measurements – both in terms of imperfections and failures loads. Then, a wider study was conducted on hot-rolled cross-sections from various classes with two different simple load cases and eventually another study was conducted to investigate the effect of the imperfection amplitude. Based on these sensitivity studies, recommendations for safe but realistic F.E. modelling (imperfection shapes and amplitudes) were given.

## References

- Cruise R.B. and Gardner L. (2006). "Measurement and prediction of geometric imperfections in structural stainless steel members." *Structural Engineering and Mechanics*; 24(1): 63-89.
- Dawson R.G. and Walker A.C. (1972). "Post-buckling of geometrically imperfect plates." *Journal of Structural division ASCE*; 98(1): 75-94.
- EN 1993-1-5 (2005). "Eurocode 3: Design of Steel Structures, Part 1-5: Plated structural elements."
- Greiner R., Kettler M., Lechner A., Jaspart J.-P., Boissonnade N., Bortolotti E., Weynand K., C. Ziller, and R. Order (2007). "RFCS Semi-Comp: Plastic member capacity of semi-compact steel sections - a more economic design." *Final report (01/01/06 - 30/06/07) - RFCS - Steel RTD (Contract RFS-CR-04044)*.

- Jandera M., Gardner L., and Machacek J. (2008). "Residual stresses in cold-formed stainless steel hollow sections." *Journal of Constructional Steel Research* 64, 1255-1263.
- Kettler M. (2008). "Elastic-Plastic Cross-Sectional Resistance Of Semi-Compact H- And Hollow Sections." PhD thesis, Technical University of Graz.
- Nseir J. (2015). "The development of a new design method for the cross-section capacity of tubular steel sections." PhD thesis, Liege University.
- Schafer B.W. and Pekoz T. (1998), "Computational modeling of cold-formed steel-characterizing geometric imperfections and residual stresses." *Journal of Constructional Steel Research*.